Z. Angew. Math. Phys. (2024) 75:21

https://doi.org/10.1007/s00033-023-02156-w

Zeitschrift für angewandte Mathematik und Physik ZAMP

Mathematical modelling of a slow flameless combustion of a two-dimensional paper

Lorenzo Fusi, Benedetta Calusi, Antonio Giovinetto and Leonardo Panconi

Abstract. We present a mathematical model for the slow combustion (smoldering) of a two-dimensional sheet of paper. We describe the evolution of the char region, and we investigate the effects of an orthogonal air flow on the shape of the combustion front. The mathematical formulation consists in a set of two nonlinear PDEs for the temperature and the oxygen concentrations coupled with one ODE for the cellulose concentration. The (dimensionless) problem is solved numerically by means of a spectral collocation scheme based on Chebyshev polynomials. Our results show that the Péclet and the Lewis number strongly influence the shape of the ignition front and that the advancement of the combustion front does not occur if advection and diffusion are neglected (zero Péclet and Lewis numbers). In particular we observe that the burning region and the ignition front are strongly influenced by the velocity of the airflow and by the mass and heat transport phenomena due to diffusion and advection. We shall see that the increasing of the ratio between the convective and diffusive characteristic times (Péclet number) and the decreasing of the ratio between the mass and heat diffusive characteristic times (Lewis number) have a "flattening effect" on the combustion front.

Mathematics Subject Classification. 35K57, 65Nxx, 65M70, 35K05.

Keywords. Smoldering, Combustion front, Mathematical modelling, PDEs, Spectral collocation methods.

List of symbols

μ^*	Oxygen molar concentration (mol/m^3)
μ_c^*	Oxygen reference concentration (mol/m^3)
ρ^*	Cellulose molar concentration (mol/m^3)
ρ_c^*	Cellulose reference molar concentration (mol/m^3)
ρ_p^*	Paper molar concentration (mol/m^3)
ρ_g^*	Air molar concentration (mol/lt)
c_p^*	Specific heat of paper (J/(mol °K))
c_g^*	Specific heat of air (J/(mol °K))
k_p^*	Heat conductivity of paper (W/(m °K))
k_g^*	Heat conductivity of air (W/(m °K))
θ	Molar fraction of the paper
$T*$	Absolute temperature of the paper (°K)
T_c*	Ignition temperature of the paper (°K)
T_a*	Ambient temperature of the paper (°K)
$\boldsymbol{V}*$	Gas speed (m/s)
$\boldsymbol{q}*$	Enthalpy flux (W/(m^2))
$\boldsymbol{x}*$	Space coordinate (m)
L^*	Length and width of the sheet (m)
t^*	Time (s)
A^*	Reaction rate function (lt/(mol s))

Published online: 16 January 2024

β^*	Reaction rate factor (°K)
λ^*	Reaction rate constant (lt/(mol s))
Γ^*	Heat production constant (reaction) (J/mol)
γ^*	Radiation constant (reaction) (W/(m^3 °K^4))
t_v^*	Oxygen advective characteristic time
t_o^*	Oxygen diffusive characteristic time
t_p^*	Oxygen consumption (due to reaction) characteristic time
t_r^*	Reaction characteristic time
t_d^*	Thermal diffusion characteristic time
t_a^*	Heat production (due to reaction) characteristic time
t_q^*	Thermal radiation characteristic time

1. Introduction

The smoldering process is a "non-flaming" mode of combustion in which the emitted gas does not glow. It is mainly governed by the availability of its basic constituents: fuel, oxidant and heat. In the slow combustion of a sheet of paper the oxygen interacts with the paper (solid fuel) to produce char, gaseous products and heat that sustains the process [1]. The system is extremely complex, involving many chemical simultaneous reactions [12], and it is further complicated by instabilities occurring at the propagation front. These instabilities, which manifest themselves in directional finger-like patterns, result from the competition between molecular transport and heat transfer [4–10,12].

Zik et al. [13] have developed a phenomenological model to predict the fingers' spacing, showing that the latter phenomenon is controlled by the Péclet number (ratio between molecular advection and diffusion). In particular, they present an experimental setup, schematically shown in Fig. 1, in which the sheet is ignited on one side and it is exposed to an airflow orthogonal to the combustion front. To build up a mathematical model, the intrinsic Hele–Shaw geometry suggests to consider a 2D model, thus extending the 1D problem studied by Fasano et al. [3] in which solutions were found in the form of traveling waves. The "Hele–Shaw geometry" is a natural geometrical setting for the problem under examination. Indeed, the thickness of the sheet of paper is far smaller than its length and width, so that we may disregard any variation along the axis perpendicular to the paper. This observation motivates the choice of a 2D setting. The experiment performed by Zik et al. [13] makes use of the airflow velocity V_{O_2} as a controllable parameter, showing that char patterns of combusted paper are formed as V_{O_2} is reduced. For sufficiently large V_{O_2}, the combustion front is essentially even, but when V_{O_2} is reduced the front becomes periodic

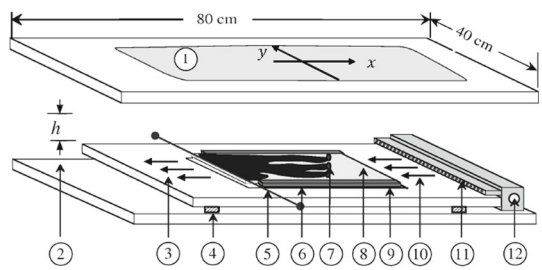

FIG. 1. Sketch of the experimental setup, from [13]: 1—glass top; 2—variable gap between top and bottom plates h; 3—outflow of combustion products; 4—spacers to control h; 5—ignition wire; 6—heat-conducting boundaries; 7—flame front; 8—fuel; 9—interchangeable bottom plate; 10—uniform flow O_2/N_2; 11—gas diffuser; 12—gas inlet. The flow direction is parallel to the x-axis

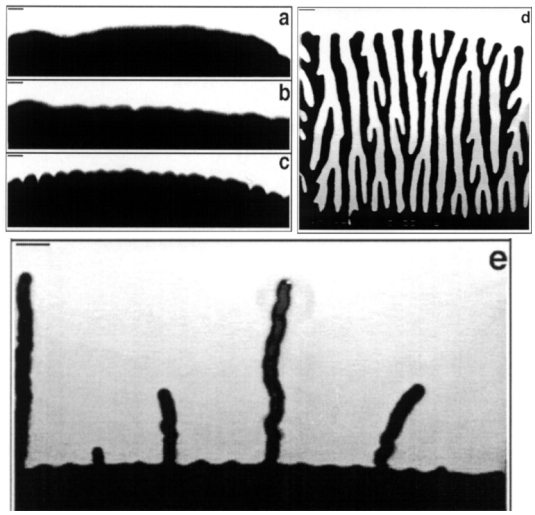

FIG. 2. Various patterns of burning paper which appear in the experiment, [13]. $V_{O_2} = 11.4$ cm/s (**a**); $V_{O_2} = 10.2$ cm/s (**b**); $V_{O_2} = 9.2$ cm/s (**c**); $V_{O_2} = 1.3$ cm/s (**d**); $V_{O_2} = 0.1$ cm/s (**e**).

and, as V_{O_2} is reduced further, the patterns exhibit fingers with tip splitting, see Fig. 2. The uniformity of the ignition front is thus strictly related to the speed of the airflow.

The scope of the present paper is to develop a mathematical model for describing the evolution of the char region and for investigating the effects of the airflow on the shape of the combustion front. We shall not deal with stability issues, which means we are not interested in studying the pattern formation. Indeed, as shown in [13], there exists a critical Péclet number below which the front becomes unstable. As the oxygen supply is reduced, small bumps along the interface begin to compete for oxygen (thermal diffusive instability) and if the oxygen flow is further decreased, these bumps consume all the oxygen available in their vicinity and separate in distinct fingers. Though our work does not study the formation of instabilities, our results highlight that the Péclet number and Lewis number (ratio between oxygen and heat diffusion) influence the shape of the combustion front. In particular, we find that the increase of the Péclet number renders the ignition front more uniform, in other words flatter, which is physically consistent with the experimental observations. The same occurs with the reduction of the Lewis number.

The model presented here is partially based on the papers by Ikeda et al. [2] (our model can be included in the one of Ikeda et al., although they do not study the problem numerically) and Fasano et al. [3] and aims at describing the propagation of the combustion front when a flow of air orthogonal to the front is applied to the paper sheet. Differently from [3], here we consider a 2D setting. The mathematical formulation consists in a set of two nonlinear PDEs for the temperature and the oxygen concentration and one ODE for the cellulose concentration. After performing a suitable scaling, the problem is put in a non-dimensional form and solved numerically. We prove that the advancement of the combustion front does not occur if advection and diffusion are disregarded (null Péclet and Lewis numbers). The 2D problem is solved by means of a spectral collocation scheme based on Chebyshev polynomials. We have chosen the spectral collocation method for its high accuracy and for the simplicity of the considered geometry. The discretized nonlinear problem is solved via Newton–Raphson method. Various boundary and initial conditions are considered, and the results are discussed and interpreted.

2. The mathematical model

The combustion reaction between the oxygen and cellulose can be written as

$$C_6H_{10}O_5 + 6O_2 \ \rightarrow 6CO_2 + 5H_2O. \tag{2.1}$$

the reaction rate being a function of the temperature. We denote[1] with $\rho^*(\boldsymbol{x}^*, t^*)$ the molar density of the cellulose, with $\mu^*(\boldsymbol{x}^*, t^*)$ the molar density of oxygen and with $T^*(\boldsymbol{x}^*, t^*)$ the absolute temperature of the paper. The flowing gas has a variable composition, and it is mainly formed by oxygen, reaction products (i.e. carbon dioxide and aqueous vapour in scheme (2.1)) and inert gases, such as N_2, that do not enter the reaction. The paper sheet is formed by cellulose and other components (such as bleach). The mass balance of oxygen can be written as

$$\frac{\partial \mu^*}{\partial t^*} + \nabla^* \cdot \underbrace{\left[\boldsymbol{V}^* \mu^* - D_\mu^* \nabla^* \mu^*\right]}_{\text{flux of oxygen}} = \alpha \frac{\partial \rho^*}{\partial t^*}, \tag{2.2}$$

where α is a non-dimensional constant that depends on the stoichiometric coefficients of reaction (2.1), $\boldsymbol{V}^*(\boldsymbol{x}^*, t^*)$ is the speed of the gas, and D_μ^* is the oxygen diffusivity coefficient (assumed to be constant). Assuming a first-order reaction for (2.1), the molar density of the cellulose $\rho^*(\boldsymbol{x}^*, t^*)$ satisfies the following equation

$$\frac{\partial \rho^*}{\partial t^*} = -A^*(T^*)\rho^* \mu^*, \tag{2.3}$$

where A^* is the reaction rate that depends on the temperature. Following Fasano et al. [3], we assume that A^* is of Arrhenius type, namely

$$A^*(T^*) = \begin{cases} \lambda^* \exp\left(-\dfrac{\beta^*}{T^* - T_c^*}\right), & T^* > T_c^*, \\ 0 & T^* \leqslant T_c^*, \end{cases}$$

where T_c^* is the ignition temperature of the cellulose (typically T_c^* is 240 ^oC) and λ^*, β^* are positive constants. We assume that the sheet can be considered as a continuous mixture in which each point is co-occupied by the gas and the cellulose in given proportions. If the velocity $\boldsymbol{V}^*$ is not large enough to remove all the heat produced by the reaction, we may safely assume that the thermal contact between the gas and the paper is perfect and we can define a cumulative density of enthalpy

$$H^* = \left[\rho_p^* c_p^* \theta + \rho_g^* c_g^* (1-\theta)\right] T^*, \tag{2.4}$$

where $\rho_p^* c_p^*$, $\rho_g^* c_g^*$ are the heat capacities of the paper and of the gas, respectively, θ is the molar fraction of the paper (constant), $(1-\theta)$ is the molar fraction of the gas. The molar fraction of the paper can be safely assumed constant if we consider that the porous structure of the paper is not significantly altered by temperature variations. Still following Fasano et al. [3], we notice that the combustion process affects only a small portion of the paper (cellulose) so that, neglecting the composition of the paper, we may consider $\rho_p^* c_p^*$ to be a constant. In the same spirit, recalling that the gas is formed by oxygen, inert gases and reaction products we can make the assumption that the variation of the components is negligible and take $\rho_g^* c_g^*$ constant. Under these hypotheses the cumulative enthalpy density can be rewritten as $H^* = \bar{\rho}^* \bar{c}^* T^*$, where the heat capacity $\bar{\rho}^* \bar{c}^* = const.$ The enthalpy flux

$$\boldsymbol{q}^* = \underbrace{-\left[k_p^* \theta + k_g^* (1-\theta)\right] \nabla^* T^*}_{\text{diffusive flux}} + \underbrace{\left[\rho_g^* c_g^* (1-\theta) T^* \boldsymbol{V}^*\right]}_{\text{advective flux}},$$

[1] Throughout the paper the starred quantities denote dimensional variables.

is written as the sum of a diffusive and a convective contribution, k_g^*, k_p^* (constant) being the heat conductivities of gas and paper, respectively. The advective flux considers only the gas, since the only admissible energy transport mechanics in the cellulose sheet is clearly diffusion. In conclusion we have

$$H^* = \bar{\rho}^* \bar{c}^* T^*, \qquad \boldsymbol{q}^* = -k^* \nabla^* T^* + \varphi^* \boldsymbol{V}^* T^*, \tag{2.5}$$

with

$$k^* = k_p^* \theta + k_g^* (1-\theta), \quad \varphi^* = \left[\rho_g^* c_g^* (1-\theta)\right]. \tag{2.6}$$

We are not going to deal with the fluid dynamics of the problem, i.e. the problem in which $\boldsymbol{V}^*$ has to be determined solving momentum balance (e.g. Darcy's flow). Indeed, in this case we should add a new variable (pressure) and take into account the thermal expansion of the gas. Even though the densities of the components of the gas can be taken independent of the pressure (subsonic flow), the dependence of these densities on the temperature of the gas should be taken into account, rendering the determination of $\boldsymbol{V}^*$ extremely difficult. To avoid this complication we assume that $\boldsymbol{V}^*$ is a given vector independent of $\boldsymbol{x}^*$ and t^*. The energy balance thus becomes

$$\bar{\rho}^* \bar{c}^* \frac{\partial T^*}{\partial t^*} + \varphi^* \boldsymbol{V}^* \cdot \nabla^* T^* - k^* \Delta T^* = \underbrace{\Gamma^* A^*(T^*) \rho^* \mu^*}_{\substack{\text{Heat production rate} \\ \text{due to reaction}}} + \underbrace{\gamma^* \left({T_a^*}^4 - {T^*}^4 \right)}_{\substack{\text{Heat transfer rate} \\ \text{due to thermal radiation}}} . \tag{2.7}$$

The first term on the r.h.s. of (2.7) represents the rate at which heat is produced by the reaction, while the second represents the heat exchange rate between the paper and the surroundings by thermal radiation. The quantities Γ^*, γ^* are positive constants, whereas T_a^* is ambient temperature. Our problem consists of equations (2.2), (2.3), (2.7) for the unknowns μ^*, ρ^*, T^*, i.e. a set of two partial differential equations plus an ordinary differential equation for the cellulose density. The domain of the problem is the square $\Omega^* = [-L^*, L^*] \times [-L^*, L^*]$. The problem must be coupled with proper initial and boundary conditions.

3. Non-dimensional formulation

We rescale the variables in the following way:

$$u = \frac{T^*}{T_c^*}, \quad p = \frac{\rho^*}{\rho_c^*}, \quad w = \frac{\mu^*}{\mu_c^*}, \quad t = \frac{t^*}{t_{ref}^*}, \quad \boldsymbol{x} = \frac{\boldsymbol{x}^*}{L^*},$$

where ρ_c^* is a reference cellulose density, μ_c^* is a reference oxygen density, T_c^* is the ignition temperature, and t_{ref}^* is a timescale to be selected. The oxygen velocity is assumed of the form $\boldsymbol{V}^* = -V^* \boldsymbol{i}$, meaning that the air flow is directed front from right to left. We introduce the characteristic times:

- $t_v^* = \dfrac{L^*}{V^*}$ oxygen advective characteristic time;
- $t_o^* = \dfrac{{L^*}^2}{D_\mu^*}$ oxygen diffusive characteristic time;
- $t_p^* = \dfrac{1}{\alpha \lambda^* \rho_c^*}$ oxygen consumption (due to reaction) characteristic time;
- $t_r^* = \dfrac{1}{\lambda^* \rho_c^*}$ reaction characteristic time;
- $t_d^* = \dfrac{{L^*}^2 \bar{\rho}^* \bar{c}^*}{k^*}$ thermal diffusion characteristic time;
- $t_a^* = \dfrac{\bar{\rho}^* \bar{c}^* T_c^*}{\lambda^* \rho_c^* \mu_c^* \Gamma^*}$ heat production (due to reaction) characteristic time;
- $t_q^* = \dfrac{\bar{\rho}^* \bar{c}^*}{{T_c^*}^3 \gamma^*}$ thermal radiation characteristic time;

Setting

$$\varphi = \frac{\varphi^*}{(\bar{\rho}^*\bar{c}^*)}, \quad \delta = \frac{T_a^*}{T_c^*} < 1,$$

we get the following non-dimensional problem

$$\begin{cases} \dfrac{\partial w}{\partial t} - \left(\dfrac{t^*_{ref}}{t^*_v}\right)\dfrac{\partial w}{\partial x} - \left(\dfrac{t^*_{ref}}{t^*_o}\right)\Delta w = -\left(\dfrac{t^*_{ref}}{t^*_p}\right)A(u)pw, \\ \dfrac{\partial p}{\partial t} = -\left(\dfrac{t^*_{ref}}{t^*_r}\right)A(u)pw, \\ \dfrac{\partial u}{\partial t} - \varphi\left(\dfrac{t^*_{ref}}{t^*_v}\right)\dfrac{\partial u}{\partial x} - \left(\dfrac{t^*_{ref}}{t^*_d}\right)\Delta u = \left(\dfrac{t^*_{ref}}{t^*_a}\right)A(u)pw + \left(\dfrac{t^*_{ref}}{t^*_q}\right)[\delta^4 - u^4], \end{cases} \tag{3.1}$$

where

$$A(u) = \begin{cases} \exp\left(-\dfrac{\beta}{u-1}\right) & u > 1, \\ 0 & u \leqslant 0, \end{cases} \qquad \beta = \frac{\beta^*}{T_c^*}. \tag{3.2}$$

System (3.1), which must be solved in $\Omega = [-1,1] \times [-1,1]$, must be coupled with initial and boundary conditions.

4. A simple case with no diffusion and no advection

Suppose $t^*_{ref} \ll t^*_v, t^*_o, t^*_d$ and $t^*_{ref} \sim t^*_p, t^*_r, t^*_a, t^*_q$. Setting

$$k = \frac{t^*_{ref}}{t^*_r}, \qquad \tau = \frac{t^*_{ref}}{t^*_a}, \qquad \xi = \frac{t^*_{ref}}{t^*_q}. \qquad \phi = \frac{t^*_{ref}}{t^*_p}, \tag{4.1}$$

problem (3.1) reduces to the following set of differential equations

$$\begin{cases} \dfrac{\partial w}{\partial t} = -\phi A(u)pw, \\ \dfrac{\partial p}{\partial t} = -kA(u)pw, \\ \dfrac{\partial u}{\partial t} = \tau A(u)pw + \xi[\delta^4 - u^4], \end{cases} \tag{4.2}$$

with initial conditions $w_o(x,y) > 0$, $p_o(x,y) > 0$, $u_o(x,y) > 0$. In this simplified situation x and y play the role of parameters. It is easy to check that, when $u_o < 1$ at some point $(x,y) \in \Omega$, the differential equation for the temperature is given, at least initially, by

$$\frac{\partial u}{\partial t} = \xi[\delta^4 - u^4], \qquad u(x,y,0) = u_o(x,y) < 1.$$

The above can be integrated between 0 and t giving

$$4t\xi\delta^3 = \ln\left[\frac{|u+\delta||u_o-\delta|}{|u-\delta||u_o+\delta|}\right] + 2\left[\arctan\left(\frac{u}{\delta}\right) - \arctan\left(\frac{u_o}{\delta}\right)\right]. \tag{4.3}$$

The solution is therefore given implicitly as $t = t(u)$. It is straightforward to see that function (4.3) has a vertical asymptote at $u = \delta$, meaning that for $t \to \infty$ the function $u \to \delta$. If $u_o \in (\delta, 1)$ the function

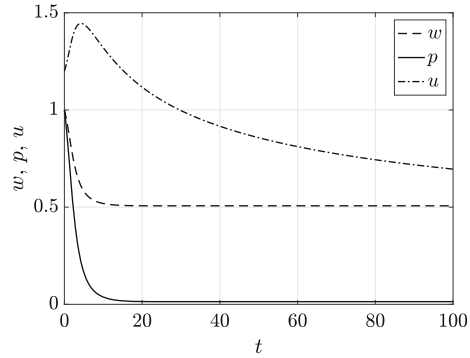

FIG. 3. No advection and diffusion. Initially increasing temperature with $u_o > 1$

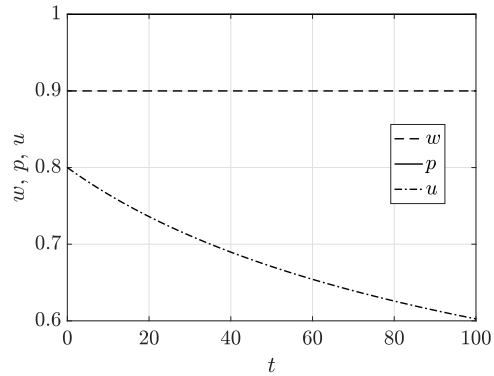

FIG. 4. No advection and diffusion. Decreasing temperature with $u_o < 1$

$u(t)$ decreases to δ; if $u_o < \delta$ the function $u(t)$ increases to δ. We may conclude that, at a point (x, y) where $u_o < 1$, the temperature can never attain the critical value $u = 1$ and hence the paper can never be burned at (x, y). This result proves that the propagation of the ignition front can be driven only by transport mechanisms such as advection or diffusion. In Fig. 3 we have reported the solution of system (4.2) with $w_o = 1$, $p_o = 1$, $u_o = 1.2$, $\phi = 1$, $k = 2$, $\tau = 1$, $\xi = 0.01$, $\delta = 0.4$, $\beta = 0.5$. The nonlinear system has been solved via spectral collocation method and exploiting Newton–Raphson algorithm. In this case, the initial temperature $u(x, y, 0) = u_o(x, y)$ is above 1 and hence the paper is already burning at (x, y). The temperature initially increases, but then decreases towards $\delta = 0.4$. Notice that when $u \leqslant 1$ (i.e. when $t \gtrsim 30$) the functions p and w become constant. In Fig. 4 we have reported the solution of system (4.2) with $w_o = 0.9$, $p_o = 1$, $u_o = 0.8$, $\phi = 1$, $k = 2$, $\tau = 1$, $\xi = 0.01$, $\delta = 0.4$, $\beta = 0.5$. In this case, the initial temperature $u(x, y, 0) = u_o(x, y)$ is below 1 and the paper is never burning at (x, y), since the temperature is always below the critical value 1. The temperature decreases towards the asymptotic value $\delta = 0.4$.

Table 1. *Non-dimensional parameters*

	Pe	Le	β	φ	ξ	k	τ	δ
D1	1	1	0.5	1	0.01	1	1	0.4
D2	10	1	0.5	1	0.01	1	1	0.4
D3	1	5	0.5	1	0.01	1	1	0.4
D4	1	1	0.5	1	0.1	1	1	0.4

5. The problem in the oxygen diffusion timescale

Here we consider the full problem with advection and diffusion. Let us select $t^*_{ref} = t^*_o$ (i.e. the timescale of oxygen diffusion). Problem (3.1) becomes

$$\begin{cases} \dfrac{\partial w}{\partial t} - \mathrm{Pe}\dfrac{\partial w}{\partial x} - \Delta w = -\phi A(u) p w, \\ \dfrac{\partial p}{\partial t} = -k A(u) p w, \\ \dfrac{\partial u}{\partial t} - \varphi \mathrm{Pe}\dfrac{\partial u}{\partial x} - \mathrm{Le}\Delta u = \tau A(u) p w + \xi[\delta^4 - u^4], \end{cases} \tag{5.1}$$

where

$$\mathrm{Pe} = \frac{t^*_o}{t^*_v}, \qquad \mathrm{Le} = \frac{t^*_o}{t^*_d}, \qquad k = \frac{t^*_o}{t^*_r}, \qquad \tau = \frac{t^*_o}{t^*_a}, \qquad \xi = \frac{t^*_o}{t^*_q}. \qquad \phi = \frac{t^*_o}{t^*_p}. \tag{5.2}$$

The numbers Pe, Le represent the Péclet number and the Lewis number, respectively. Problem (5.1) is solved numerically by a spectral collocation method based on Chebyshev polynomials, see [11]. The system is spatially discretized on a $(N+1)\times(N+1)$ 2D Gauss–Lobatto grid, $N = 40$. The differential operators in system (5.1) are replaced by discretized operators built through the differentiation matrices

$$\frac{\partial}{\partial x} \approx \mathbb{I} \otimes \mathrm{D}, \qquad \frac{\partial}{\partial y} \approx \mathrm{D} \otimes \mathbb{I},$$

where $\mathbb{I}$ is the $(N+1)\times(N+1)$ identity matrix, D is the differentiation matrix defined in chapter 6 of [14], and $\otimes$ is the Kronecker product between matrices. System (5.1) is thus transformed into an algebraic nonlinear system that includes the boundary conditions. We use spectral differentiation in space and finite differences in time (Euler explicit) with time step $dt = 10^{-2}$. At each time step the nonlinear system is solved via Newton–Raphson method (quadratic convergence) in which iterations are terminated when the error tolerance is of the order of 10^{-14}. To investigate the behaviour of the ignition front together with its dependence on the material parameters, we consider different boundary and initial conditions.

5.1. Numerical results and discussion

We begin by considering

$$\begin{cases} \left.\dfrac{\partial u}{\partial x}\right|_{x=\pm1} = \left.\dfrac{\partial u}{\partial y}\right|_{y=\pm1} = 0, \qquad \left.\dfrac{\partial w}{\partial x}\right|_{x=\pm1} = \left.\dfrac{\partial w}{\partial y}\right|_{y=\pm1} = 0, \qquad w\Big|_{x=1} = 1, \\ u_o = (1-x^2)^2(1-y^2)^2 + 0.8, \qquad p_o = 1, \qquad w_o = 1, \end{cases} \tag{5.3}$$

with non-dimensional groups reported in Table 1.

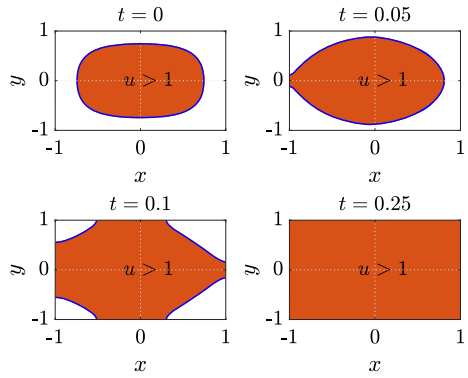

FIG. 5. Burning region (orange) for (5.3) with parameters set D1 of Table 1

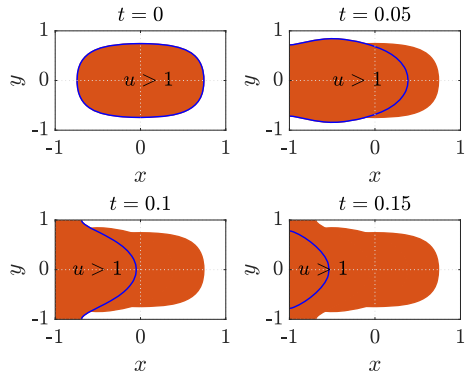

FIG. 6. Burning region (orange) for (5.3) with parameters set D2 of Table 1

The initial condition u_o in (5.3) is chosen so that the inner part of the paper sheet is initially burning, while the outer part is not. The boundary conditions for w and u are such that the diffusive flux is zero on the boundary $\partial\Omega$ except at $x = 1$ where w is given. Compatibility conditions between the initial and boundary data at $t = 0$ are satisfied.

To investigate the convergence we have considered $dt = 0.01$ and analysed the solution at time $t = 0.2$ for increasing N. In particular we have taken the sup norm of the solution $\|(u, w, p)\|_\infty$ (time is fixed; the norm is with respect to the spatial coordinates). We report in the table the sup norm for increasing N with $dt = 0.01$ at time $t = 0.2$ (a further reduction of the time step dt does not significantly change the norm). The data are the ones of case D1 in Table 1 with initial and boundary conditions (5.3).

N	$\|(u, w, p)\|_\infty$
5	1.151772
10	1.182135
20	1.182792
30	1.183845
40	1.183887
50	1.183889

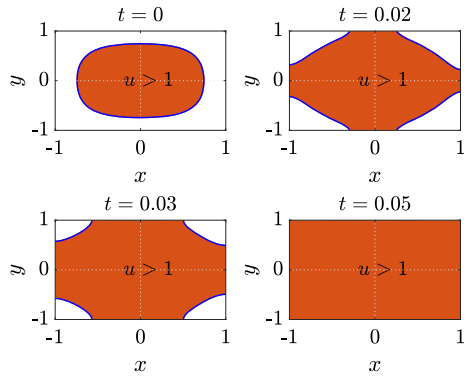

FIG. 7. Burning region (orange) for (5.3) with parameters set D3 of Table 1

In Fig. 5 we show the evolution of the burning region for initial and boundary data (5.3) where the parameters are those of D1 of Table 1. In this case the complete burning is reached at $t = 0.25$. In Fig. 6 we show the evolution of the burning region for D2. In this case, we notice that at each time t the region where the temperature is above 1 (burning) does not necessarily contain the ones in which $u > 1$ at previous times, meaning that for fixed time t the burning domain is a juxtaposition of the burning domains at earlier times (a sort of envelope of the burning domains).

In Figs. 7, 8 we show the evolution of the boundary region for parameters D3, D4. In all of these plots we have indicated the part of the cellulose in which temperature is above the critical value 1. As one can easily notice, the burning region comprehends also parts in which the temperature is below 1. Indeed, once a part of the domain is burning, it remains so even if the temperature drops below the ignition point 1.

Looking at Figs. 5–8 we see that the increase of Pe produces a reduction of the region where $u > 1$ (see Figs. 5, 6), i.e. the combustion front travels much faster because of the increase of V_{O_2}. If we now look at Figs. 5, 7 we notice that the increase of Le results in a reduction of the time needed to burn the whole paper (a large Le means a large supply of oxygen). Finally the increase of ξ (increase of radiative heat loss, see Figs. 7, 8) produces a reduction of the burning area, since part of the heat needed to burn the paper is lost due to radiation at a higher speed. The same type of behaviour is evident from Figs. 9–12 (different types of boundary and initial conditions).

We remark that the initial conditions in (5.3) (and the others that we shall consider further on) are completely arbitrary. In case (5.3) we have an initial condition in which the burning domain resembles an ellipse. The right boundary condition for the oxygen concentration is prescribed oxygen concentration $w = 1$. Hence the balance between the consumption rate of oxygen and the inlet flux must adapt in order to guarantee that the oxygen concentration remains 1 at $x = 1$. If we look, for instance at Fig. 8, i.e. case D4, the combustion front initially advances, but after some time it starts to recede towards the left (stationary state). The stationary state is independent of the initial conditions (that state is dictated only by the boundary conditions), while the way the stationary state is reached depends on the initial conditions. If we change the initial conditions of the system with data D4 and ICs, BCs (5.3), we change the contours at initial times, but for times larger or equal to 1 the contour is more or less the same. We have to bear in mind that we are not simulating a specific case with parameters taken from experiments; we are only interested in seeing the effects that the non-dimensional groups have on the combustion front. The initial data that we choose are indeed completely arbitrary and do not reflect a real initial state.

In order to see the influence of the initial and boundary conditions on the evolution of the burning region, we consider other types of initial and boundary conditions. As for (5.3), these conditions are completely arbitrary and do not reflect any real initial data.

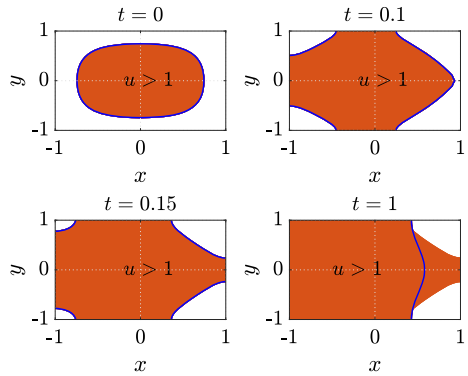

FIG. 8. Burning region (orange) for (5.3) with parameters set D4 of Table 1

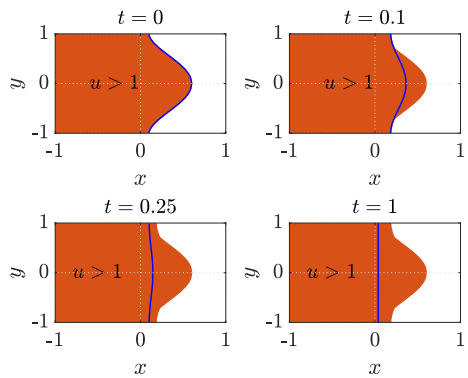

FIG. 9. Burning region (orange) for (5.4) with parameters set D1 of Table 1

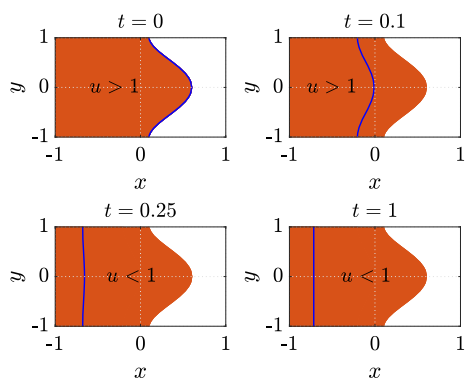

FIG. 10. Burning region (orange) for (5.4) with parameters set D2 of Table 1

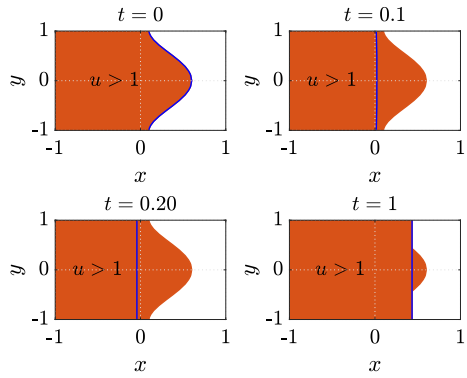

FIG. 11. Burning region (orange) for (5.4) with parameters set D3 of Table 1

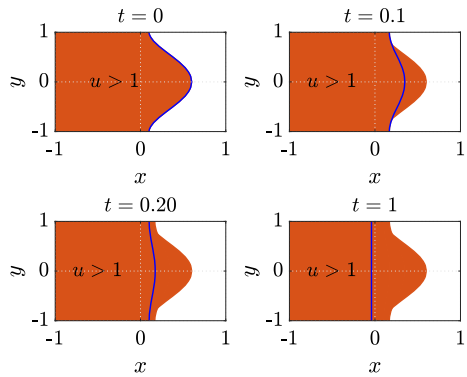

FIG. 12. Burning region (orange) for (5.4) with parameters set D4 of Table 1

In Figs. 9, 10, 11, 12 we show the evolution of the burning region for initial and boundary conditions (5.4). In this case the initial temperature u_o is such that the left part of the paper is burning, while the right part is not. The boundary conditions for w are such that the overall flux is null on $x = -1$, $y = \pm 1$ with a prescribed overall oxygen flux at $x = 1$. The temperature at the left border $x = -1$ is an initially increasing function of time that starts to decay at time $t = 1$. On the right boundary $x = 1$ we impose the ambient temperature. In this case the compatibility conditions at $x = \pm 1$ and $t = 0$ are not satisfied. Figures 9, 10, 11, 12 correspond to the set of parameters D1, D2, D3, D4, respectively.

$$\begin{cases} \left.\dfrac{\partial u}{\partial y}\right|_{y=\pm 1} = 0, \qquad \left. u \right|_{x=-1} = 1 + 5te^{-t}, \qquad \left. u \right|_{x=1} = \delta, \\ \left.\left[\mathrm{Pe}w + \dfrac{\partial w}{\partial x}\right]\right|_{x=-1} = 0, \qquad \left.\left[\mathrm{Pe}w + \dfrac{\partial w}{\partial x}\right]\right|_{x=-1} = 1, \qquad \left.\dfrac{\partial w}{\partial y}\right|_{y=\pm 1} = 0, \\ u_o = 0.5(1-y^2)^2 + (1.1 - x), \qquad p_o = 1, \qquad w_o = 1. \end{cases} \tag{5.4}$$

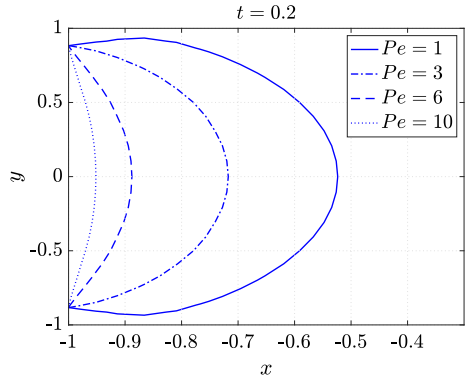

FIG. 13. Ignition front at $t = 0.2$ with different Péclet for (5.5) and data D1 (except Péclet) of Table 1

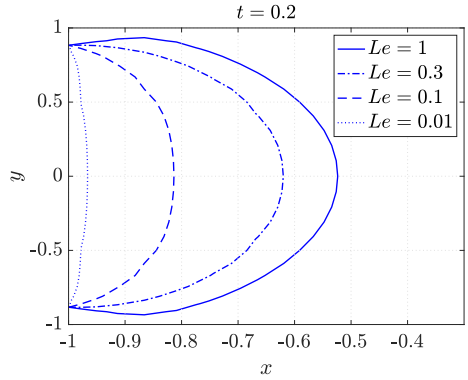

FIG. 14. Ignition front at $t = 0.2$ with different Lewis for (5.5) and data D1 (except Lewis) of Table 1

$$\begin{cases} \left.\dfrac{\partial u}{\partial y}\right|_{y=\pm 1} = 0, \qquad \left. u\right|_{x=-1} = 0.99 + t(1-y^2)^2, \qquad \left. u\right|_{x=1} = \delta, \\ \left[\mathrm{Pe}w + \dfrac{\partial w}{\partial x}\right]\Big|_{x=-1} = 0, \qquad \left[\mathrm{Pe}w + \dfrac{\partial w}{\partial x}\right]\Big|_{x=-1} = 1, \qquad \left.\dfrac{\partial w}{\partial y}\right|_{y=\pm 1} = 0, \\ u_o = 0.99, \qquad p_o = 1, \qquad w_o = 1. \end{cases} \tag{5.5}$$

$$\begin{cases} \left.\dfrac{\partial u}{\partial y}\right|_{y=\pm 1} = 0, \qquad \left. u\right|_{x=-1} = 0.99 + t\Big(\sin(\pi y^2)\Big)^2, \qquad \left. u\right|_{x=1} = \delta, \\ \left[\mathrm{Pe}w + \dfrac{\partial w}{\partial x}\right]\Big|_{x=-1} = 0, \qquad \left[\mathrm{Pe}w + \dfrac{\partial w}{\partial x}\right]\Big|_{x=-1} = 1, \qquad \left.\dfrac{\partial w}{\partial y}\right|_{y=\pm 1} = 0, \\ u_o = 0.99, \qquad p_o = 1, \qquad w_o = 1. \end{cases} \tag{5.6}$$

Finally, to better illustrate the effects of the Péclet and Lewis numbers on the ignition front $u = 1$, we have considered initial and boundary data (5.5), (5.6) plotting the level sets $u = 1$ for various values

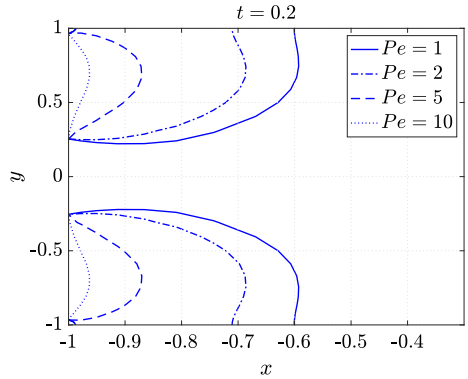

FIG. 15. Ignition front at $t = 0.2$ with different Péclet for (5.6) and data D1 (except Péclet) of Table 1

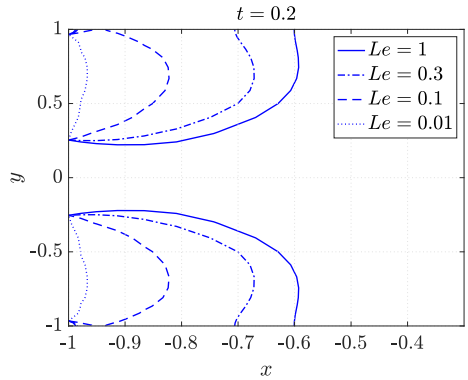

FIG. 16. Ignition front at $t = 0.2$ with different Lewis for (5.6) and data D1 (except Lewis) of Table 1

of Pe and Le at time $t = 0.2$, see Figs. 13, 14, 15, 16. The set of data (5.5), (5.6) are practically identical except for the temperature at $x = -1$. In (5.5) the boundary condition for u at $x = 1$ is of polynomial type, while in (5.6) is trigonometric. In both cases the initial temperature of the paper is constant and below the ignition point. Once again, the compatibility conditions at $x = \pm 1$ are not satisfied. Looking at Figs. 13, 14, 15, 16, we notice that the increase of Pe has a "flattening" effect on the curve $u = 1$. This is consistent with the experimental observations of Zik et al [13] (even though the diverse pattern there are due to instabilities), where the authors show that, for "large" airflow velocity, the propagation front is almost flat (see Fig. 2*a*). The same "flattening" effect is obtained by reducing the Lewis number, i.e. when the characteristic time of oxygen diffusion becomes smaller than the characteristic diffusive time of heat.

6. Conclusions

In this paper we have investigated the propagation of the combustion front (smoldering) of a two-dimensional cellulose sheet when an orthogonal flow of oxygen is laterally applied. The model is partially based on the works by Ikeda et al. [2] and Fasano et al. [3]. Differently from most of the numerical papers on smoldering here we have considered a two-dimensional setting, i.e. a two-dimensional sheet of paper that can be subjected to a series of boundary conditions.The mathematical model consists in a set of two

nonlinear PDEs for the temperature and the oxygen concentrations and one ODE for the cellulose concentration. We have solved the corresponding non-dimensional problem numerically through a spectral collocation scheme based on Chebyshev polynomials. We have used spectral differentiation in space and Euler explicit in time, showing the convergence of the method. The discretized nonlinear problem has been solved via Newton–Raphson method. We have proved that the propagation of the combustion front does not occur when Pe, Le $= 0$, i.e. when transport mechanisms such as advection and diffusion are neglected. Moreover, when the full problem with advection and diffusion is considered, we have shown that an increase of the Péclet number leads to a more uniform ignition front, a phenomenon consistent with the physical observations reported in Zik et al. [13]. On the other hand, by decreasing of the Lewis number, we have obtained the same "flattening" effect. A natural extension of this work would be the study of the formation of instability patterns and the influence of the airflow on this phenomenon.

We have proved that, depending on the initial and boundary data, the increase of Pe may result in a reduction of the region where $u > 1$, meaning that the combustion front travels much faster because of the increase of airflow velocity V_{O_2}. We have also proved that increase of Le may produce a reduction of the time needed to burn the whole paper (large Le means a large supply of oxygen). Finally, we have seen that the increase of ξ, i.e. the increase of radiative heat loss, produces a reduction of the burning area, because a part of the heat needed to burn the sheet is lost due to radiation

Acknowledgements

The present work has been performed under the auspices of the Italian National Group for Mathematical Physics (GNFM-Indam).

Funding Open access funding provided by Università degli Studi di Firenze within the CRUI-CARE Agreement.

References

[1] Aldushin, A.P., Matkowsky, B.J.: Instabilities, fingering and the Saffman–Taylor problem in filtration combustion. Combust. Sci. Technol. **133**(4–6), 293–341 (1999)
[2] Ikeda, K., Mimura, M.: Mathematical treatment of a model for smoldering combustion. Hiroshima Math. J. **38**(3), 349–361 (2008)
[3] Fasano, A., Mimura, M., Primicerio, M.: Modelling a slow smoldering combustion process. Math. Methods Appl. Sci. **33**(10), 1211–1220 (2010)
[4] Gorman, M., El-Hamdi, M., Pearson, B., Robbins, K.A.: Ratcheting motion of concentric rings in cellular flames. Phys. Rev. Lett. **76**(2), 228 (1996)
[5] Kuwana, K., Kushida, G., Uchida, Y.: Lewis number effect on smoldering combustion of a thin solid. Combust. Sci. Technol. **186**(4–5), 466–474 (2014)
[6] Kuwana, K., Suzuki, K., Tada, Y., Kushida, G.: Effective Lewis number of smoldering spread over a thin solid in a narrow channel. Proc. Combust. Inst. **36**(2), 3203–3210 (2017)

[7] Ijioma, E.R., Muntean, A., Ogawa, T.: Effect of material anisotropy on the fingering instability in reverse smoldering combustion. Int. J. Heat Mass Transf. **81**, 924–938 (2015)
[8] Kagan, L., Sivashinsky, G.: Pattern formation in flame spread over thin solid fuels. Combust. Theor. Model. **12**(2), 269–281 (2008)
[9] Moallemi, M.K., Zhang, H., Kumar, S.: Numerical modeling of two-dimensional smoldering processes. Combust. Flame **95**(1–2), 170–182 (1993)
[10] Nave, O.: Analysis of the two-dimensional polydisperse liquid sprays in a laminar boundary layer flow using the similarity transformation method. Adv. Model. Simul. Eng. Sci. **2**, 1–15 (2015)
[11] Canuto, C., Hussaini, M.Y., Quarteroni, A., Zang, T.A.: Spectral Methods: Fundamentals in Single Domains. Springer, New York (2007)
[12] Sivashinsky, G.I.: Instabilities, pattern formation, and turbulence in flames. Annu. Rev. Fluid Mech. **15**(1), 179–199 (1983)
[13] Zik, O., Olami, Z., Moses, E.: Fingering instability in combustion. Phys. Rev. Lett. **81**(18), 3868 (1998)
[14] Trefethen, L.N.: Spectral methods in MATLAB. Society for industrial and applied mathematics (2000)

Lorenzo Fusi, Benedetta Calusi, Antonio Giovinetto and Leonardo Panconi
Dipartimento di Matematica e Informatica “U.Dini”
Universitá degli studi di Firenze
Viale Morgagni 67/a
50134 Florence
Italy
e-mail: lorenzo.fusi@unifi.it

Benedetta Calusi
e-mail: benedetta.calusi@unifi.it

Antonio Giovinetto
e-mail: antonio.giovinetto@unifi.it

Leonardo Panconi
e-mail: leonardo.panconi@stud.unifi.it

(Received: May 15, 2023; revised: November 7, 2023; accepted: November 23, 2023)